Plastic deformation of polycrystalline alumina introduced by scaled-down drop-weight impacts

James Wade[$], Stuart Robertson, Ying Zhu, Houzheng Wu[*]

Department of Materials, Loughborough University, Leicestershire, LE11 3TU, UK

Abstract

We present our findings after scaled-down drop-weight tests, performed under relatively low loading conditions and employing a small-scale spherical indenter as a projectile, to boost the strain rate and energy density of the impact, resulted in the generation of a cavity of measurable depth on the surface of a pure, fully dense, alumina ceramic. We demonstrate that activated dislocations are a main contributor in the formation of the residual impression with an estimated maximum density of ~4.02×10^{14} m^{-2}.

Key Words: polycrystalline alumina; dislocations; plastic deformation; drop-weight impact.

1. Introduction

Since Longy and Cagnoux's paper demonstrating that, along with the fragmentation, dislocations/twins are activated during high-velocity impacts [1], a handful of researchers have paid specific attention to the role that plastic deformation plays in the performance of armour ceramics under various high-impact loading conditions [1-10]. In these investigations,

*Corresponding author: Tel: +44 15092 23342; Fax: +44 1509 223949; E-mail: h.wu2@lboro.ac.uk (H. Wu)

$ Current affiliation: Department of Mechanical, Aeronautical and Civil Engineering, The University of Manchester, Manchester, M13 9PL, UK. Contact details: Tel: +44 16130 62352; Email: james.wade@manchester.ac.uk

several methods, including gas gun tests [2], flyer plate impact tests [1,3-5] and split Hopkinson pressure bar tests [6, 7], were employed. The principle of each of these experiments is the utilisation of a high-velocity projectile/bar (100-800 ms^{-1}) in order to achieve a peak internal stress beyond the Hugoniot elastic limit, a stressing condition necessary for the initiation of dynamic plasticity [4]. From a practical standpoint, the adoption of such extreme conditions is often a financially costly, labour-intensive and lengthy process. Consequently, despite the potential findings that could be extracted from the data, many researchers and engineers do not typically evaluate plasticity in ceramics under dynamic impact conditions. Ultimately, this limits the scope of the work performed on applications involving dynamic impacts in ceramics. In addition to the cost and time constraints, the resultant impacts from the aforementioned experimental techniques frequently lead to catastrophic failure of the tested specimen. This invariably means that post-impact characterisation requires some form of reconstructive fragment analysis [10], leading to difficulties in interpreting the data. As a result, to date, the analysis of the plastic deformation in armour ceramics has not been understood to a level whereby the conditions of such a physical process and its potential impact on the dynamic/ballistic contact damage resistance of ceramic structures can be clearly defined.

The objective of the present work is to demonstrate the potential of low-velocity drop-weight (DW) impact tests as a simple, convenient and repeatable technique for studying plasticity in ceramics subjected to dynamic impacts. In doing so, we aim to expose a phenomenon after recent DW tests performed on fully-dense monolithic alumina ceramics generated a crater of marked depth and a residual damage zone far beyond anything produced by comparable quasi-static indentation tests. Despite similar DW setups and other “dynamic indentation” tests being performed by other workers [11-13], this response of the material remains

undocumented. We believe that, once instrumented, such a method could be useful in helping us understand dynamic damage in different ceramics, as well as provide a viable method for screening armour, aerospace and dentistry ceramics for better performance in advanced ceramic research.

Experimental Procedure

The alumina test samples were prepared as follows. Ultra-fine, 99.99% pure α-Al_2O_3 powder (TM-DAR, Taimei, Japan) was first ball-milled in butanol (Sigma Aldrich, USA) for 24 hrs. This slurry was then dried, crushed and ground, followed by sieving. The resultant powder was then die-pressed at ~65 MPa, to form a 40 mm diameter disc with an approximate thickness of 12 mm. These discs were subsequently placed in an isostatic-press at ~200 MPa, followed by sintering in a box furnace. The sintering profile included a ramp rate of 5°C/min from room temperature to 1050°C, dwelled for 10 hrs, then to 1400°C, dwelled for 4 hrs. As shown in Fig. 1(a), this produced a 99.5% dense ceramic with an equiaxial grain structure and an average grain size of 1.38±0.73 μm. The sintered alumina samples were then polished using a 1 μm diamond abrasive before DW tests were conducted.

The DW tests themselves were performed using a 2 mm tungsten carbide (WC) ball. A photograph of the testing apparatus used is presented in Fig. 2(a). Prior to DW testing, the unconfined alumina sample was positioned directly on top of a securely fastened thick alumina block (~50 mm thick) and held in place using vacuum grease. For each test, a weighted load of 0.6 kg (5.88 N) was released from a height of ~0.5 m along rails, giving an estimated velocity of ~3.13 ms^{-1}. In this study, a total of 5 single hit tests were performed at different sites across one sample (~30 mm in diameter and ~10 mm in thickness). All test site

locations were evenly distributed around the middle of the sample with a separating distance of ~10 mm. This is ~20 times larger than the diameter of the resultant crater size, typically 0.5 mm for this impact load. We believe the aforementioned clearance between each test site was large enough to ensure an independent response in the ceramic during each impact. Frames from a high-speed camera video, taken on a HyperVision HPV-1 (Shimadzu, Kyoto, JPN) at 20,000 frames per second, demonstrates the DW process in Fig. 2(b-e), showing the indenter impacting the surface and the generation of a crater. Strain rate estimations of these impacts, assuming an initial contact diameter of 0.2 mm on impact, indicate that a falling speed of 3.13 ms^{-1} can give a peak strain rate along the surface of $>10^4$ s^{-1}, which is around the upper boundary for Hopkinson bar tests [14]. The total kinetic energy (KE) applied on contact is calculated at 2.94 J. This is a relatively low value compared with gas gun tests (10-150 J) and ballistic tests (500-4500 J). However, the benefit of having less KE to dissipate is that the residual damage zone remains intact with limited fracturing, making thorough post-testing analysis possible. In order to measure the geometry of the residual impressions produced, a 3D optical microscope (NewView 5000, Zygo Corp., USA) was used to compose 3D surface plots of the individual impressions.

Further post-impact analysis of the impressions involved examination under SEM (Leo 1530 VP, Carl Zeiss, Oberkochen, GER) and optical microscope (DMRX, Leica, Wetzler, GER). Meanwhile, lattice plastic deformation was detected and quantified using Cr^{3+}/Al_2O_3 fluorescence spectroscopy across a single impact site. Fluorescence microscopy was performed using a true confocal Raman microscope (Horiba, Japan) over a spectrum of 14,250 to 14,550 cm^{-1} with a 633 nm red line He-Ne laser. A 50× objective lens was used in conjunction with a confocal setup that involved two 50 μm pinhole apertures at 90° to one another. This provided an approximate beam diameter on the specimen surface of 1 μm and

ensured that data was only taken from the near-surface. A step size of 25 μm was used for measurements taken over ¼ of the impression. Each scan was made twice at each point for 10 s and then averaged, giving a total detection time of 20 s. In order to comparatively quantify the degree of R1 peak broadening and peak shifting, multiple measurements were taken over the polished surface of the alumina sample to serve as a reference.

3. Results and Discussion

Figure 3(a) shows a 3D surface map of one of the impressions generated during a DW impact test. By evaluating the extracted profiles of the 5 different impressions generated, we calculated an average depth of 1.21±0.15 μm and an average diameter of 475.2±18.7 μm. Notice the limited standard deviation for each value, exemplifying the high repeatability of the tests.

Analysis of the fracture patterns produced during the DW impact tests exhibited in Fig. 2(b) highlights a number of key features. Firstly, extensive ring-cracking is observed, the formation of which can be explained by adapting Hertzian indentation fracture mechanics. Here, ring-cracks are activated by surface flaws/defects in a well-defined tensile stress field just outside the boundary of contact [15]. Amongst these ring-cracks are multiple radial cracks emanating through and away from the initial point of contact. In a study by Evans and Wilshaw performing overloaded quasi-static Hertzian indentation tests, it was suggested that such cracks are a strong indicator of the onset of plastic deformation [16]. Located in areas surrounding the residual impression are what we describe as large arching-cracks. As shown, these cracks can be up to 700 μm away from the cavity boundary, are very deep and appear to be the initial stages of some form of fragmentation. Based on such observations, we conclude

that these cracks did not form under Hertzian contact because they do not have a centre point aligned with that of the point of initial contact, show no signs of subsurface cone-cracking, and are located well-beyond any area of physical contact. At present, the mechanism by which these arching-cracks nucleate and propagate is unknown. However, we are curious as to how such large cracks could develop so far away from the point of physical contact in these dynamic impacts. Finally, there is no indication of significant micro-cracking, particularly inside the ring-cracked region underneath the point of initial contact. This is confirmed in Fig. 3(c) by the lack of grain dislodgement in the cross-sectioned and polished impression that one would expect with the coalescence of grain boundary micro-cracking. Based on the evidence presented, it would appear that the residual impression must be attributable to the plastic response of the Al_2O_3 and is not a consequence of micro-crack based pseudo-ductility through grain boundary sliding, as has been documented after similar blunt contacts in alumina under quasi-static loading conditions [17].

Further evidence to support this can be seen in Fig. 4(a), where the R1 peak in a fluorescence spectrum taken from a highly-strained site near the cavity edge exhibits significant broadening compared to that at the polished surface. A comparative quantification of this data reveals a discernible increase of 6.8 cm^{-1} in the full width half maximum (FWHM). By adopting the model of Wu *et al* [18], we can convert this value into the dislocation density, in this case estimated at 4.02×10^{14} m^{-2}.

In-plane fluorescence mapping results in Fig. 4(b), covering a quarter of the same impression and depicting the FWHM, highlight a ring or ‘band’ of broadening peaks, with a radius of ~200 µm. This is located inside the cavity boundary. Here, the alumina has experienced

significant mechanically-induced plastic deformation during the DW test, activating dislocation densities in the order of 10^{14} m^{-2}.

As shown in Fig. 4(c), complementary fluorescence mapping of the cross-sectioned impression presented in Fig. 3(c), reveals that the band of broadening at the surface is only part of a highly deformed region beneath the contact interface, where the maximum broadening is found to be along the contact axis and ~125 μm below the surface. Here, the maximum ΔFWHM of 5.79 cm^{-1}, equating to a dislocation density of ~2.80×10^{14} m^{-2}, is a value consistent with the broadening peaks in Fig. 3(b). According to Lawn, the maximum shear stress under quasi-static Hertzian contact should be located at ≈0.5*a* [19], where *a* is the radius of contact. By using the average measured diameter of the cavity (475.2 μm) as the diameter of contact, 2*a*, the location of the maximum shear stress in an idealised Hertzian shear stress field would be at ~118.8 μm below the surface. This result is consistent with the ~125 μm depth at which the maximum broadening is observed. From the point of maximum broadening, plastic deformation then expands outwardly, with dislocation densities gradually degrading with distance. Incidentally, this trend fits well with the contours of principal shear stress presented in Fig. 4.5 of Johnson [20]. It is worth noting that whilst the shear stress field endured during DW tests appears to resemble that of Hertzian indentation, the scale of the permanent deformation exhibited is unprecedented in this form of quasi-static testing at the low loads employed during the DW impact tests.

4. Conclusion

In summary, we have characterised residual impressions generated on the surface of pure, fully dense alumina after scaled-down, blunt contact DW impact tests. The formation of such

cavities, with an average measured depth of 1.21±0.15 μm, was found to coincide with extensive fracture damage in the form of ring-cracks, radial cracks, and large macro-scale arching-cracks that appear to be exclusive to the dynamic loading of a blunt indenter. How these arching-cracks originate is unknown at this point. Fracture analysis of the subsurface revealed no micro-crack-induced grain boundary sliding as a contributing factor in the generation of an impression. Instead, quantification of any plastic deformation through fluorescence mapping showed that there was a band of dislocations within the cavity boundary and a region of extensive dislocations located directly underneath the point of contact. By measuring the broadening of Cr^{3+}/Al_2O_3 fluorescence peak, we have determined the dislocation density to be in the order of 10^{14} m^{-2}. Given the low loads employed in these tests compared to those used in its quasi-static equivalent, such high dislocation densities and increased deformation in the DW impressions were considered to be a consequence of the dynamic effect. However, detailed analysis of the mechanics is needed in a further study.

References

1. Longy F, Cagnoux K. Plasticity and microcracking in shock-loaded alumina. J Am Ceram Soc 1989;76:971-9.
2. Dancer CEJ, Curtis HM, Bennett SM, Petrinic N, Todd RI. High strain rate indentation-induced deformation in alumina ceramics measured by Cr^{3+} fluorescence mapping. J Eur Ceram Soc 2011;31:2177-87.
3. Louro L, Meyers M. Effect of stress state and microstructural parameters on impact damage of alumina-based ceramics. J Mater Sci 1989;24:2516-32.
4. Chen MW, McCauley JW, Dandekar DP, Bourne NK. Dynamic plasticity and failure of high-purity alumina under shock loading. Nat Mater 2006;5:614-618.

5. Mukhopadhyay AK, Joshi KD, Dey A, Chakraborty R, Rav A, Biswas SK, Gupta SC. Shock deformation of coarse grain alumina above Hugoniot elastic limit. J Mater Sci 2010;45:3635.
6. Lankford J. Compressive strength and microplasticity in polycrystalline alumina. J Mater Sci 1977;12:791-6.
7. Lankford J, Predebon WW, Staehler JM, Subhash G, Pletka BJ, Anderson CE. The role of plasticity as a limiting factor in the compressive failure of high strength ceramics. Mech Mater 1998;29:205-18.
8. Merala TB, Chan HW, Howitt DG, Kelsey PV, Korth GE, Williamson RL. Dislocation microstructures in explosively deformed hard materials. Mater Sci Eng A 1988;105/106:293-8.
9. McGinn JT, Klopp RW, Shockey DA. Deformation and comminution of shock loaded α-Al_2O_3 in the Mescall zone of ceramic armor. Mat Res S C 1994;362:61.
10. Wu HZ, Ghosh S, Dancer CEJ, Todd RI. Ballistic damage in alumina ceramics – Learning from the fragments. In: LaSalvia JC, editors. Advances in Ceramic Armor V, Hoboken, New Jersey: Wiley & Sons, Inc; 2014, p. 49-62.
11. Sherman D, Brandon DG. The ballistic failure mechanism and sequence in semi-infinite supported alumina tiles. J Mater Res 1997;12:1335-43.
12. Brennan RE, Green WH, Sands JM. Destructive testing and non-destructive evaluation of alumina structural ceramics. In: Swab JJ, Singh D, Salem S, editors, Advances in Ceramic Armor V, Hoboken, New Jersey: Wiley & Sons, Inc; 2009, p. 135-46.
13. Subhash G, Maiti S, Geubelle PH, Ghosh D. Recent advances in dynamic indentation fracture impact damage and fragmentation of ceramics. J Am Ceram Soc 2008;91:2777-91.

14. Fields JE, Walley, SM, Proud, WG, Goldrein HT, Siviour CR. Review of experimental techniques for high rate deformation and shock studies. J Impact Engng 2004;30:725-75.
15. Warren PD. Determining the fracture toughness of brittle materials by Hertzian indentation. J Eur Ceram Soc 1995;15:201-7.
16. Evans AG, Wilshaw TR. Quasi-static solid particle damage in brittle solids-I. Observations analysis and implications. Acta Metall 1976;24:939-56.
17. Guiberteau F, Padture NP, Lawn BR. Effect of grain size on Hertzian contact damage in alumina. J Am Ceram Soc 1994;77:1825-31.
18. Wu HZ, Roberts SG, Derby B. Residual stress distributions around indentations and scratches in polycrystalline Al_2O_3/SiC nanocomposites measured using fluorescence probes. Acta Mater 2008;56:140.
19. Lawn BR. Indentation of ceramics with spheres: A century after Hertz. J Am Ceram Soc 1998;81:1977-94.
20. Johnson KL. Contact mechanics. Cambridge University Press, 1985.

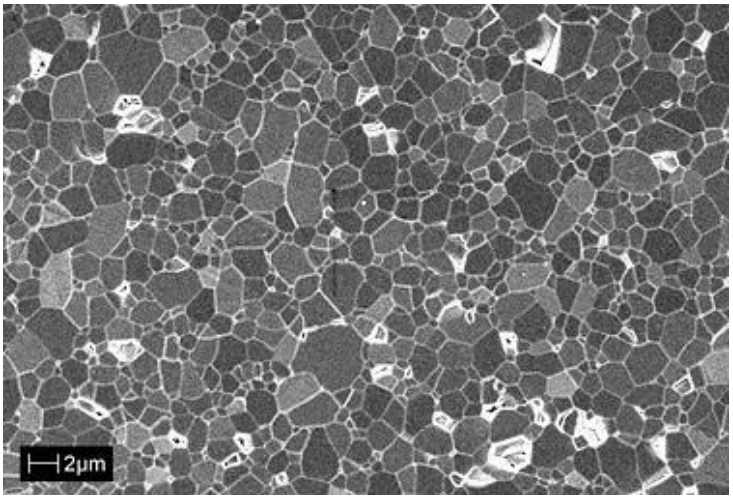

Fig. 1. SEM micrograph of the alumina microstructure after 1 µm polishing and thermal etching.

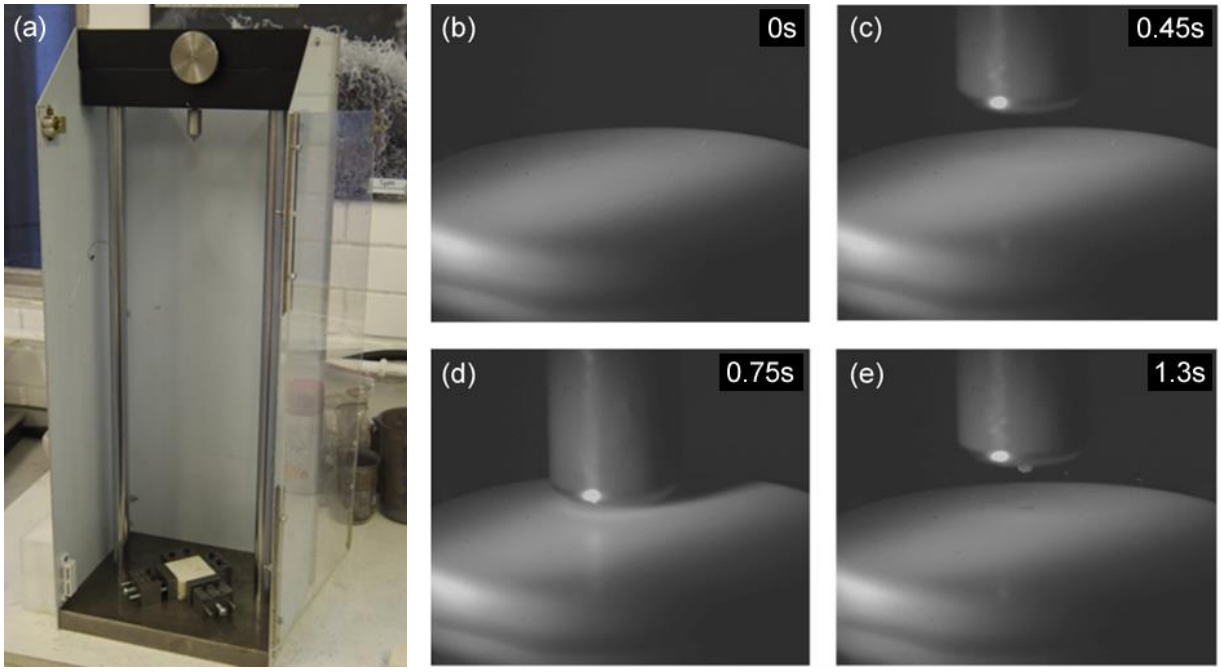

Fig. 2. The DW test apparatus; (a) a photograph of the DW test rig, (b-e) frames taken from high-speed camera footage of the DW impact process; (b) shows the sample prior to damage; (c) at 0.45s the impacting head comes into view, this is travelling at 3.13 ms^{-1}; (d) at 0.75s the blunt indenter hits the surface with an impact energy density of ~94 MJ/m^2 (assuming a 0.2 mm contact diameter); (e) at 1.3s the load bounces back leaving the residual impression generated on the samples surface.

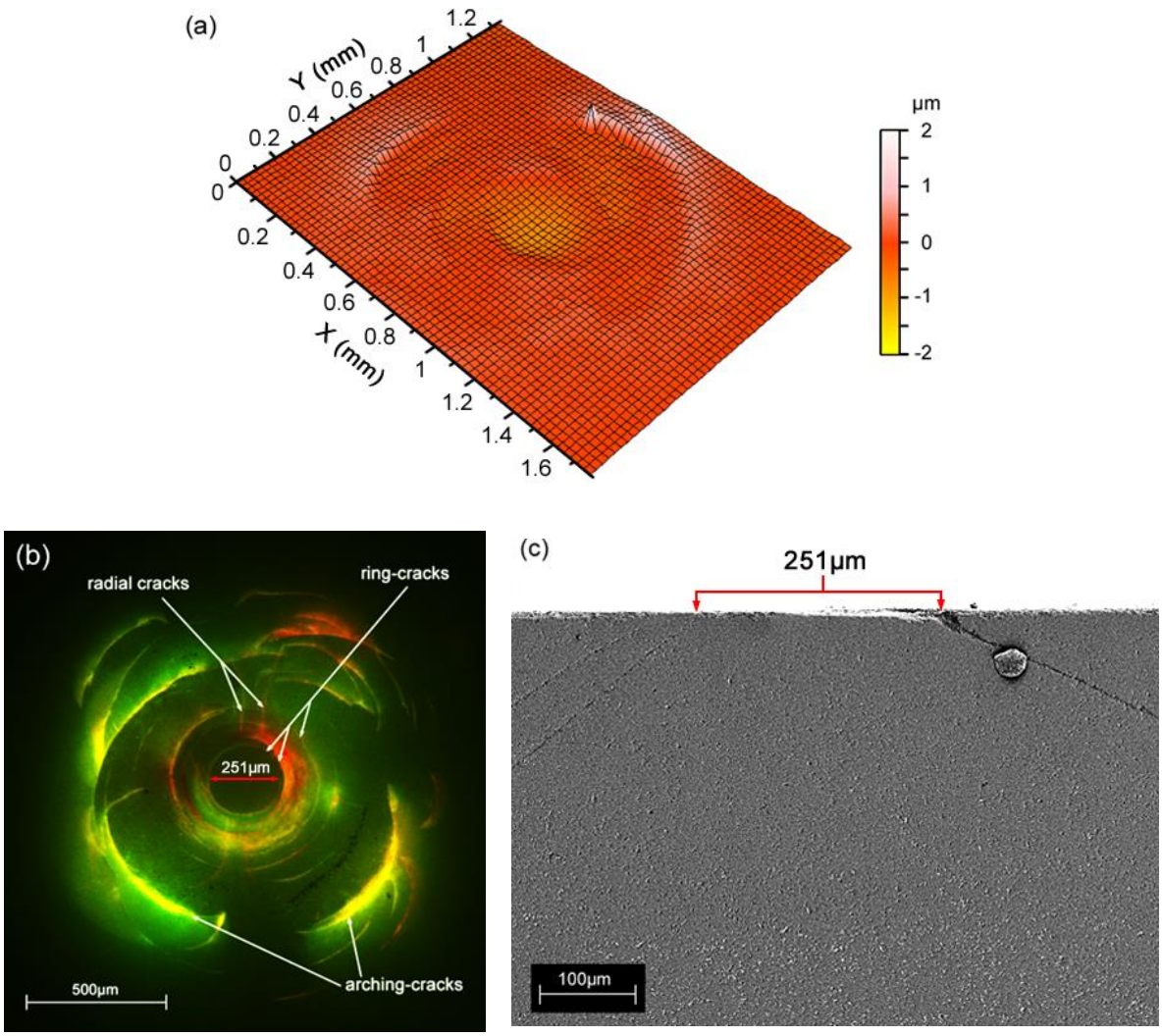

Fig. 3. Optical and SEM imaging of the deformation and damage produced during a 0.6kg DW impact test on alumina: (a) 3D optical microscopy map of the residual impression, (b) UV optical microscopy of the resultant fracture patterns, (c) SEM image of the cross-sectioned DW impression.

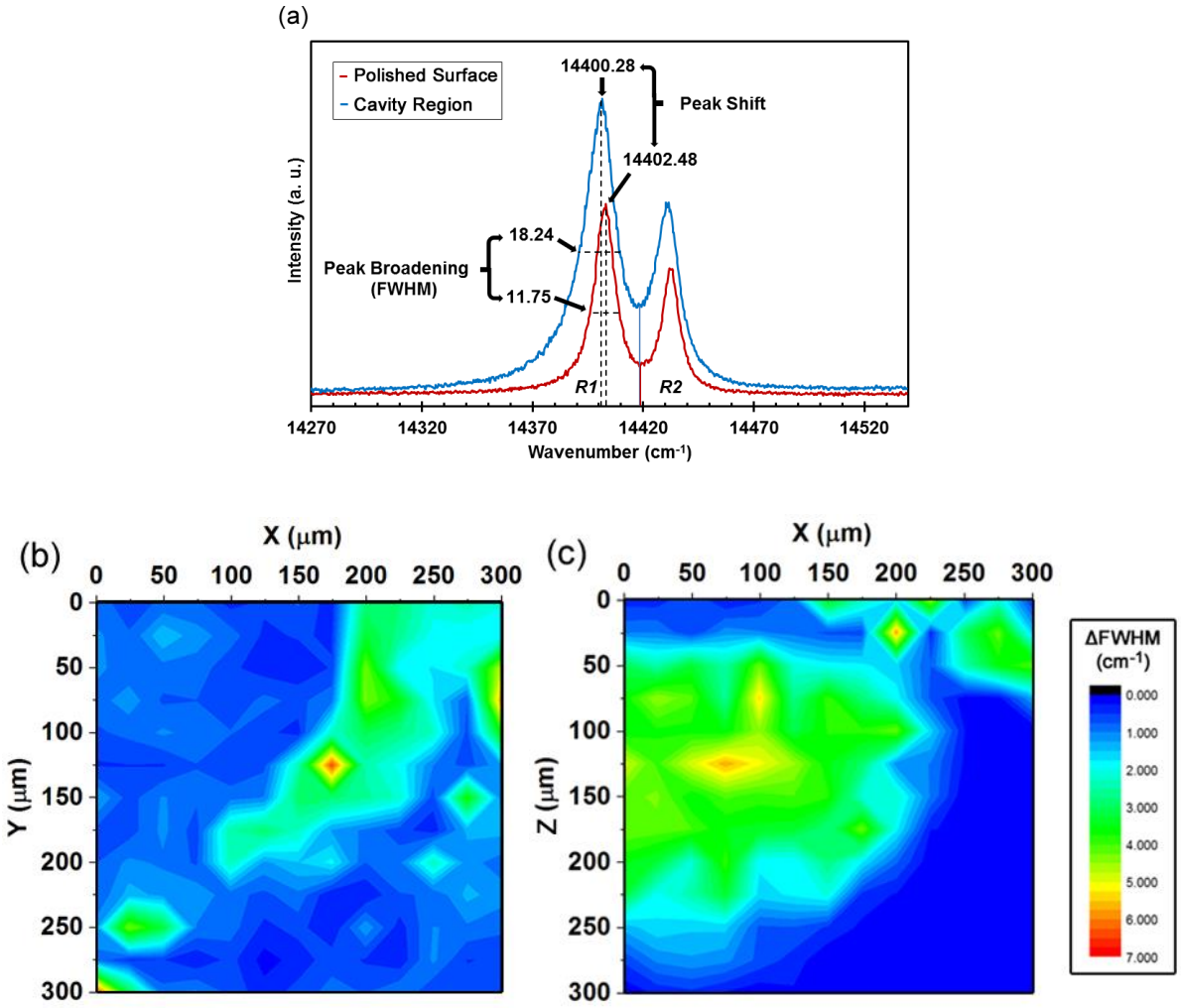

Fig. 4. Measurements of broadening (FWHM) in Cr^{3+} fluorescence spectrums around a 0.6 kg DW impression: (a) fluorescence spectra acquired from a single position on the as-polished surface (red line) and the as-impacted surface (blue line), showing the net broadening (ΔFWHM) induced by DW impact; (b) 2D map of ΔFWHM over a quarter of the in-plane surface of the impression; (c) 2D map of ΔFWHM over half of the cross-section of the impression. The (0,0) coordinate represents the centre of the impression.